ISSN 1674-1056
http://cpb.iphy.ac.cn
http://iopscience.iop.org/cpb
中国物理 B
Chinese Physics
中国物理 Chinese Physics B

# Photodetectors based on inorganic halide perovskites: Materials and devices

Ying Li(李营), Zhi-Feng Shi(史志锋), Xin-Jian Li(李新建), Chong-Xin Shan(单崇新)

**Citation:**Chin. Phys. B . 2019, 28(1): 017803. **doi:** 10.1088/1674-1056/28/1/017803
Journal homepage: http://cpb.iphy.ac.cn; http://iopscience.iop.org/cpb

**What follows is a list of articles you may be interested in**

---

## Recent research process on perovskite photodetectors:A review for photodetector – materials, physics, and applications

Yan Zhao(赵岩), Chenglong Li(李成龙), Liang Shen(沈亮)

Chin. Phys. B . 2018, 27(12): 127806. **doi:** 10.1088/1674-1056/27/12/127806

## Influence of carrier gas $H_2$ flow rate on quality of p-type GaN epilayer grown and annealed at lower temperatures

Shuang-Tao Liu(刘双韬), Jing Yang(杨静), De-Gang Zhao(赵德刚), De-Sheng Jiang(江德生), Feng Liang(梁锋), Ping Chen(陈平), Jian-Jun Zhu(朱建军), Zong-Shun Liu(刘宗顺), Wei Liu(刘炜), Yao Xing(邢瑶), Li-Yuan Peng(彭莉媛), Li-Qun Zhang(张立群), Wen-Jie Wang(王文杰), Mo Li(李沫)

Chin. Phys. B . 2018, 27(12): 127803. **doi:** 10.1088/1674-1056/27/12/127803

## Effect of depositing PCBM on perovskite-based metal-oxide-semiconductor field effect transistors

Su-Zhen Luan(栾苏珍), Yu-Cheng Wang(汪钰成), Yin-Tao Liu(刘银涛), Ren-Xu Jia(贾仁需)

Chin. Phys. B . 2018, 27(4): 047208. **doi:** 10.1088/1674-1056/27/4/047208

## Engineering of electronic and optical properties of ZnO thin films via Cu doping

Zhang Guo-Heng, Deng Xiao-Yan, Xue Hua, Xiang Gang

Chin. Phys. B . 2013, 22(4): 047803. **doi:** 10.1088/1674-1056/22/4/047803

## Effects of rapid thermal annealing on the morphology and optical properity of ultrathin InSb film deposited on $SiO_2$/Si substrate

Li Deng-Yue, Li Hong-Tao, Sun He-Hui, Zhao Lian-Cheng

Chin. Phys. B . 2013, 22(2): 027802. **doi:** 10.1088/1674-1056/22/2/027802

---

TOPICAL REVIEW — Photodetector: Materials, physics, and applications

# Photodetectors based on inorganic halide perovskites: Materials and devices*

Ying Li(李营)[1], Zhi-Feng Shi(史志锋)[1,†], Xin-Jian Li(李新建)[1], and Chong-Xin Shan(单崇新)[1,2,‡]

[1] School of Physics and Engineering, Zhengzhou University, Zhengzhou 450001, China

[2] State Key Laboratory of Luminescence and Applications, Changchun Institute of Optics, Fine Mechanics and Physics, Chinese Academy of Sciences, Changchun 130033, China

(Received 7 October 2018; revised manuscript received 12 November 2018; published online 30 December 2018)

The newly emerging metal halide perovskites have attracted considerable attention due to their exceptional optoelectronic properties. This upsurge was initially driven when the power conversion efficiency of perovskite-based photovoltaic devices exceeded 23%. Due to their optoelectronic properties, perovskite materials have also been used in light-emitting diodes, photodetectors, lasers, and memory devices. This study comprehensively discusses the recent progress of all-inorganic perovskite-based photodetectors, focusing on their structures, morphologies of their constituent materials, and diverse device architectures that improve the performance metrics of these photodetectors. A brief outlook, highlighting the main existing problems, possible solutions to these problems, and future development directions, is also provided herein.

**Keywords:** perovskites, all-inorganic, photodetectors, lead-free

**PACS:** 78.40.Fy, 72.40.+w, 85.60.Gz **DOI:** 10.1088/1674-1056/28/1/017803

## 1. Introduction

Photodetectors that convert incident optical signals to electrical signals are crucial in a broad range of applications, including medial analysis, security surveillance, optical communications, and biological sensing.[1–5] Commercialization prospects are high for photodetectors with good responsivity, fast response speed, low power consumption, good stability, and low processing cost. Among the various semiconductor materials explored for light detection, the newly emerging organic–inorganic hybrid perovskites ($CH_3NH_3PbX_3$, $X$ = Cl, Br, and I) have triggered considerable attention[6–16] probably owing to their excellent properties such as tunable bandgap, high and well-balanced electron/hole mobility, large carrier diffusion length, and low-temperature processing technique.[4,17–21] At present, most of the studied photodetectors are based on conventional semiconductors, such as graphene, two-dimensional (2D) materials, and silicon, which are expensive and require precise preparation techniques. In contrast, metal halide perovskite-based photodetectors can be fabricated with high crystallinity via solution processing at low temperatures. In addition, the device performances of perovskite photodetectors have rapidly improved over the past three years. The responsivity and specific detectivity of perovskite photodetectors can reach $10^9$ A/W and $> 10^{16}$ Jones, respectively,[22] which are higher than those of 2D materials, graphene, and commercial silicon. For example, graphene possesses high-speed broadband photodetection properties but is disadvantaged by low photoresponsivity, detectivity, and very low external quantum efficiency originating from the relatively low light absorption coefficient and the fast carrier recombination rate. Consequently, the practical optoelectronic applications of pristine graphene are rather limited.[23–25] Several problems, particularly the instability and toxicity of organic–inorganic hybrid perovskites, still remain unaddressed. Given that organic–inorganic hybrid perovskites are sensitive to oxygen and moisture, devices based on these materials would become unstable under oxygen exposure or damp conditions. This is the main obstacle to reliable device operation and potential applications of hybrid perovskite materials. As a promising alternative approach, all-inorganic lead–halide perovskites $CsPbX_3$ ($X$ = I, Br, and Cl) have recently attracted considerable attention. The first all-inorganic halide perovskites were synthesized by Protesescu *et al.* in early 2015.[26,27] Apparently, these inorganic materials possess an intrinsically higher melting point ($> 500$ °C)[28] and better photostability, earmarking them as alternative candidates for future optoelectronic applications. However, these perovskite materials contain lead, which is highly toxic and hinders the further application of these materials. After numerous theoretical and experimental efforts to screen suitable perovskites, a few promising candidates have been identified. Although the remarkable achievements of organic–inorganic perovskite-based photodetectors in optoelectronics have been

*Project supported by the National Science Foundation for Distinguished Young Scholars of China (Grant No. 61425021) and the National Natural Science Foundation of China (Grant Nos. U1604263, 11774318, and 11604302).

†Corresponding author. E-mail: shizf@zzu.edu.cn

‡Corresponding author. E-mail: cxshan@zzu.edu.cn

© 2019 Chinese Physical Society and IOP Publishing Ltd 

extensively reviewed,[29–36] a summary of all-inorganic perovskite photodetectors has not yet been published.

This study summarizes the recent achievements in all-inorganic halide perovskite-based photodetectors, including Pb-based and lead-free photodetectors. The structural feature of halide perovskites and their various synthesis methods are introduced first. Then, all-inorganic perovskite photodetectors with metal–semiconductor–metal and heterojunction structures are reviewed. Finally, this review concludes with a summary and a positive outlook on the future development of perovskite photodetectors.

## 2. Structural features and synthesis of all-inorganic perovskites

### 2.1. Structural features

Inorganic metal halide perovskites are chemically represented as $ABX_3$, where $A$ is an inorganic cation (e.g., Cs), $B$ denotes the metal cation (e.g., Pb, Sn), and $X$ is a halide anion (Cl, Br, and I).[37] A typical perovskite crystal has a cubic ($\alpha$ phase) unit cell (Fig. 1). The cation $B$ (at the center) is framed by six $X$ anions (occupying the face centers) and 12 $A$ cations (occupying the cube vertices). Eight octahedra of the $B$ halide are centralized at $B$, which can be tilted or rotated by replacement with different halide ions to adjust the material's bandgap. The crystal phase of $ABX_3$ depends on the synthesis temperature. For example, the $CsPbI_3$ structure changes from orthorhombic to cubic at 328 °C. Similarly, $CsPbBr_3$ undergoes orthorhombic-to-tetragonal phase transition at 88 °C and develops a cubic structure at 130 °C. The structural phase-transition temperatures of $CsPbCl_3$ are relatively low (the monoclinic–orthorhombic, orthorhombic–tetragonal, and tetragonal–cubic transitions occur at 37 °C, 42 °C, and 47 °C, respectively). The cubic structures of these three inorganic lead–halide perovskites are stable at high temperatures.

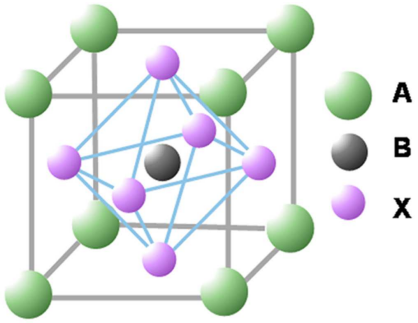



**Fig. 1.** General crystal structure of perovskites $ABX_3$.[37]

Compared with organic–inorganic hybrid perovskites, all-inorganic perovskites have received less attention, although their properties are comparable to those of organometallic perovskites. Both these materials are imbued with a direct bandgap, tunable emission wavelength, high light absorption coefficient (up to $10^5$ $cm^{-1}$), simple processing technique, as well as high and well-balanced carrier-transport ability. Regarding the tunable bandgap, perovskite photodetectors are considered as broadband detectors, enabling full-band coverage of the ultraviolet and visible light regions. The bandgap of perovskites can be tuned by varying the composition of the constituent halide ions and/or cations without changing the electronic properties of the perovskites. In the past few years, compositional tunability has been extensively studied in perovskite materials.[26,38,39]

### 2.2. Synthesis of all-inorganic perovskites

In optoelectronic devices, metal halide perovskites are mainly applied as light absorbers. Devices with excellent optoelectronic properties require high-quality perovskites, regardless of their shape and dimensions. Several synthetic methods for synthesizing halide perovskites have proliferated and they are now divisible into three main categories.

#### 2.2.1. Solution-processed synthesis

As a simple and low-cost synthesis method, one-step spin coating is commonly used to prepare perovskites with different morphologies, such as films, nanowires, nanoplatelets, and single crystals. Figure 2 schematizes the solution-processed preparation procedure of perovskite thin films, in which two precursors are mixed to form the completed absorber.[40] Herein, the synthesis of $CsPbBr_3$ is briefly described. First, CsBr is mixed with $PbBr_2$ in dimethyl sulfoxide to form the perovskite precursor solution. The $CsPbBr_3$ thin films are then prepared by spin coating the precursor solution under a low-speed spinning setting (500 rpm for 6 s) followed by a fast-speed spinning setting (4000 rpm for 30 s). Finally, to improve the coverage of the film, the solvent is evaporated by drying at 100 °C for 10 min under a nitrogen atmosphere. Li *et al.* reported a photodetector based on a $CsPbBr_3$ thin film fabricated using the one-step method, which delivered high responsivity.[41] Liu *et al.* demonstrated flexible high-performance photodetectors based on the $CsPbBr_3$/ZnO heterostructure. Their photodetectors were prepared using a solution-processed method and exhibited remarkable photodetection capabilities.[42] Tong *et al.* fabricated $CsBi_3I_{10}$ thin films by spin coating CsI and $BiI_3$ solution.[43] Another effective synthesis technique is in situ solution deposition. Applying this method, Liu *et al.* dipped the spin-coated $PbBr_2$ film into CsBr solution for several minutes and obtained high-performance $CsPbBr_3$ thin films after annealing.[44]

The solution process yields perovskite thin films, as well as high-quality nano- and micro-structures such as $CsPbCl_3$ nanocrystals.[45] Liu *et al.* reported all-inorganic

photodetectors based on solution-processed scattered $CsPbBr_3$ nanoplatelets. The nanoplatelets were highly oriented, with an average lateral dimension as large as 5 μm. Their x-ray diffraction peaks corresponded to the (001) and (002) diffractions of the orthorhombic $CsPbBr_3$ phase, and their sharpness confirmed their high crystallinity. The cross-sectional profile of the $CsPbBr_3$ nanoplatelets is indicated by the straight white line in Fig. 3(a). The lateral dimension of $CsPbBr_3$ nanoplatelets is ∼ 10 μm with 376-nm thickness.[46] Saidaminov *et al.* synthesized single millimeter-sized crystals of $CsPbBr_3$ perovskite using a low-temperature, solution-based phase-selective method. Figure 3(b) shows a semitransparent ($\sim 3 \times 2 \times 1$) $mm^3$ crystal grown in 3 h. Their study elucidated the main optical and charge transport properties of $CsPbBr_3$ crystals and demonstrated their potential for self-powered optoelectronics.[47]

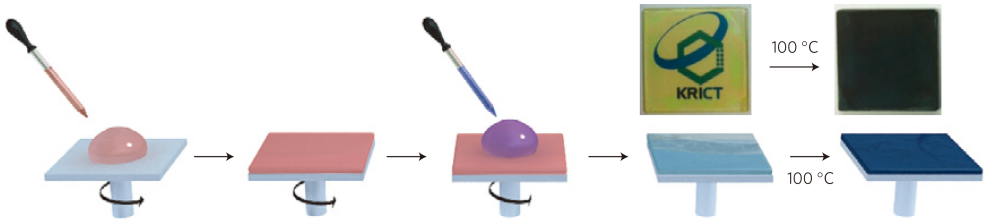



**Fig. 2.** Solvent engineering procedure for fabricating uniform and dense perovskite films.[40]

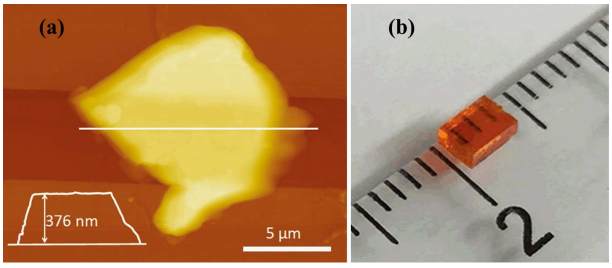



**Fig. 3.** (a) Atomic force microscopy image of a single multilayered $CsPbBr_3$ nanoplatelet bridging two metal electrodes.[46] (b) Photograph of a $CsPbBr_3$ single crystal.[47]

### 2.2.2. Vapor-assisted solution process

Chen *et al.* exploited the separate advantages of vapor and solution processes and developed a hybrid technique, known as the vapor-assisted solution process, for solar cell applications. In this method, a $PbI_2$ layer deposited by spin coating is subsequently treated with the desired $CH_3NH_3I$ vapor (Fig. 4).[48] Applying the same process, Wang *et al.* reported a visible-blind ultraviolet photodetector based on $CH_3NH_3PbCl_3$ thin film. First, a $PbCl_2$ thin film is deposited via thermal evaporation; then, an upper $CH_3NH_3Cl$ thin film is developed via spin coating, and finally, the $CH_3NH_3PbCl_3$ film is formed via annealing.[49] The vapor-assisted solution process is mainly used for fabricating perovskite thin film with a high surface coverage, which are desired in hybrid perovskite solar cells.[50–55] All-inorganic perovskites are rarely prepared using this method.

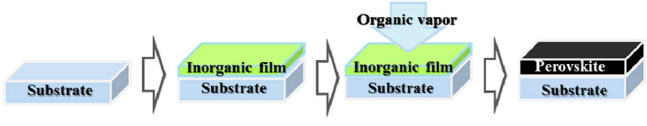



**Fig. 4.** Schematic of the vapor-assisted solution process.[48]

### 2.2.3. Vapor deposition

Vapor-phase synthesis is suitable for growing epitaxial nanostructures of inorganic perovskites with improved crystal quality because crystals grown using this method are thermally stable at moderately high temperatures.[55–57] Figure 5 schematizes the vapor deposition setup.[58] Thin films of dense and compact perovskites can be obtained using this method. Snaith *et al.* optimized the ratio between the organic cation (methylammonium iodide, $CH_3NH_3I$) and $PbCl_2$, thereby obtaining the best composition for perovskite thin-film formation via vapor evaporation.[59] To ensure a high-purity product, Malinkiewicz *et al.* prepared the perovskite layers via sublimation in a high-vacuum chamber.[60] Most films prepared via vapor deposition are hybrid perovskites used in solar cells.[61–66] In contrast, nano- and micro-structures prepared via vapor deposition are widely used in photodetectors. Chen *et al.* reported a vapor-phase epitaxial growth of horizontal single-crystal $CsPbX_3$ ($X$ = Cl, Br, and I). They formed nanowires and microwires with controlled crystallographic orientations on the (001) plane of phlogopite and muscovite mica and fabricated them into $CsPbBr_3$ networks with photoluminescence waveguiding and good photodetection performance. These well-connected $CsPbBr_3$ nanowires could serve as straightforward platforms for fundamental studies and optoelectronic applications.[55]

At present, solution-processed synthesis, vapor-assisted solution process, and vapor deposition are all widely and successfully employed in perovskite preparation. Among these




**Fig. 5.** Schematic of the vapor deposition process.[58]

three methods, solution-processed synthesis is low-cost, easier to operate, and obtains a high-quality perovskite layer at relatively low temperatures. The vapor-assisted solution process is more complicated compared with the solution method but is suitable for materials that do not easily dissolve in solvents. Vapor-phase synthesis obtains epitaxial perovskite micro/nanostructures with high crystal quality. Moreover, the dimensions and thicknesses of crystals grown using this method are easily controlled.

#### 2.2.4. Hot-injection approach

Perovskite photodetectors can be fabricated using a quantum dots (QDs) solution prepared via the hot-injection method. Following the traditional hot-injection approach, which is a common synthesis method of metal chalcogenide QDs, Kovalenko *et al.* synthesized the first monodispersed $CsPbX_3$ QDs with a high degree of compositional bandgap engineering.[26] Therein, the Cs precursors were injected into the lead–halide precursors containing hot solvents with high boiling points. A mixture of oleic acid and oleylamine dissolved the lead–halide sources and stabilized the QDs. In situ PL measurements revealed a very fast reaction process after the Cs precursor injection. Most $CsPbX_3$ QDs were synthesized within a few seconds. In such a rapid synthesis method, the unit size of the $CsPbX_3$ QDs strongly depends on the reaction temperature and is reduced by decreasing the reaction temperature. In that study, the $CsPbX_3$ QDs were produced with a tunable size of 4–15 nm.

## 3. Lead–halide perovskite photodetectors

### 3.1. Parameters of photodetectors

Photodetectors are evaluated using several important parameters, such as responsivity ($R$), detectivity ($D^*$), external quantum efficiency (EQE), response time, and linear dynamic range (LDR), which are briefly described as follows:

**Responsivity ($R$)** This parameter defines the photocurrent generated per unit power of the incident light on the effective area of a photodetector. It is usually expressed as follows:

$$R = \frac{I_\mathrm{p} - I_\mathrm{d}}{P_\mathrm{opt} \cdot S}, \tag{1}$$

where $I_\mathrm{d}$ is the dark current, $P_\mathrm{opt}$ is the incident light intensity, and $S$ is the effective illuminated area. $R$ reflects the photoelectric conversion capability of the photocurrent.

**Detectivity ($D^*$)** This parameter characterizes the weakest light level detectable by the device. $D^*$ is determined by the responsivity and noise of a photodetector, which is defined as follows:

$$D^* = \frac{(A\Delta f)^{1/2} \cdot R}{i_\mathrm{n}}, \tag{2}$$

where $A$ is the effective area of the detector, $\Delta f$ is the electrical bandwidth, and $i_\mathrm{n}$ is the noise current. When the dark current is dominated by shot noise, $D^*$ is represented as follows:

$$D^* = \frac{A^{1/2} \cdot R}{(2eI_\mathrm{d})^{1/2}}, \tag{3}$$

where $I_\mathrm{d}$ is the dark current. Clearly, the dark current should be reduced as far as possible to distinguish very weak optical signals.

**External quantum efficiency (EQE)** The EQE is defined as the number ratio between the outputted electron–hole pairs and the incident photons per unit time. It is expressed as follows:

$$\mathrm{EQE} = \frac{I_\mathrm{p}/e}{P_\mathrm{opt}/h\nu}, \tag{4}$$

where $e$ is the elementary charge, $h$ and $c$ are the Planck's constant and light speed, respectively, and $\nu$ and $\lambda$ denote the frequency and wavelength of the incident light, respectively.

**Response time** The temporal photoresponse is a critical evaluation parameter of optoelectronic devices. The response speed is represented by the rise and fall times of the current ($t_\mathrm{r}$ and $t_\mathrm{f}$, respectively). $t_\mathrm{r}$ ($t_\mathrm{f}$) defines the rising (falling) time from 10% (90%) to 90% (10%) of the maximum current.

**Linear dynamic range (LDR)** Another merit measure of photodetectors is the LDR or photosensitivity (typically quoted in dB). Within the LDR, the $I_\mathrm{p}$ is linearly related to the incident light intensity. The LDR is expressed as follows:

$$\mathrm{LDR} = 20\log\frac{I_\mathrm{p}}{I_\mathrm{d}}, \tag{5}$$

where $I_\mathrm{p}$ is the photocurrent measured at a light intensity of 1 mW/cm$^2$ and $I_\mathrm{d}$ is the dark current.

### 3.2. Metal–semiconductor–metal (MSM) photodetector

The sensitivity of organic–inorganic halide perovskites to oxygen exposure and damp conditions destabilizes the corresponding devices; therefore, all-inorganic lead halide perovskites, chemically represented by $CsPbX_3$ ($X$ = I, Br, and Cl), have received considerable research attention. The simplest configuration for $CsPbX_3$ photodetector fabrication is metal–semiconductor–metal (MSM), which sandwiches the perovskite absorber between two contact electrodes. This structure is widely adopted in perovskites photodetectors.[67–71] Li *et al.* fabricated prototypical $CsPbBr_3$ thin-film photodetectors with a coplanar MSM interdigitated patterned Au-electrode configuration. The $CsPbBr_3$ thin film was prepared using one-step spin coating (Fig. 6) and exhibited a compact structure and good optical properties. The photocurrent ratio, responsivity, specific detectivity, EQE, and response speed of the as-designed photodetectors were extremely high ($1.06\times10^5$, 55 A/W, $0.9\times10^{13}$ Jones, 16700%, and 430/318 μs, respectively). Results demonstrated the uniqueness and effectiveness of the all-inorganic $CsPbBr_3$ perovskite thin film in photodetector applications, while providing a simple and low-cost method for visible light optical sensor productions.[41]

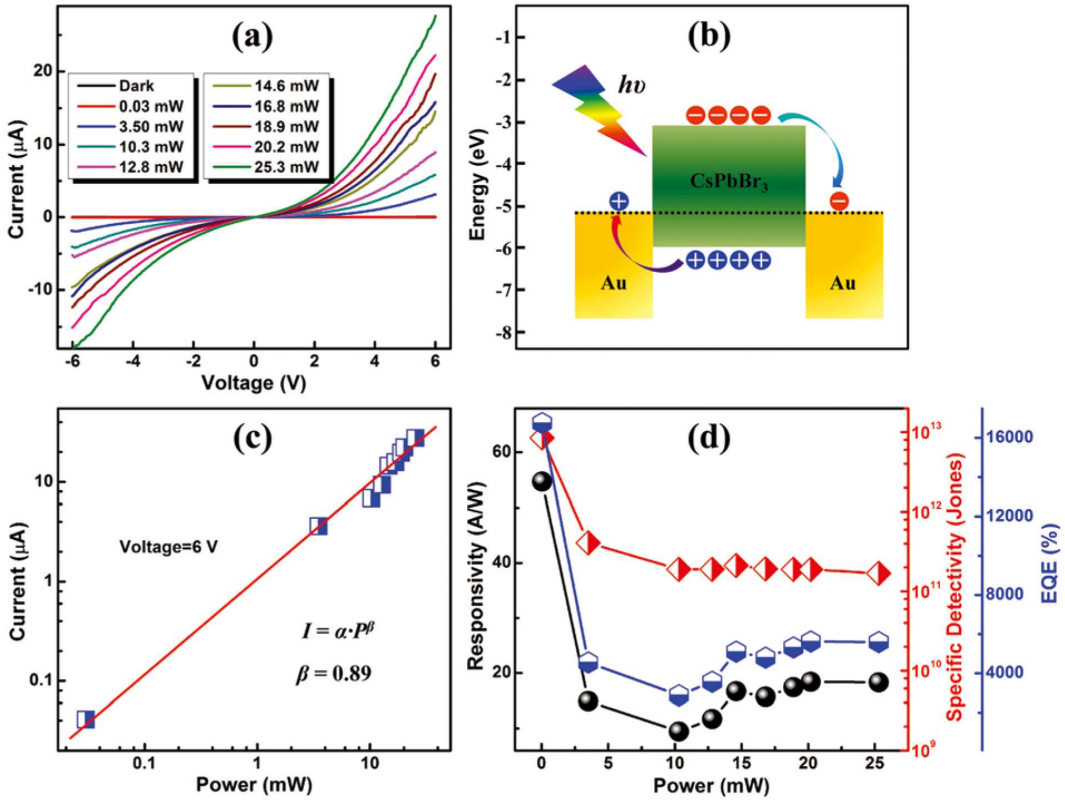



**Fig. 6.** (a) Current–voltage ($I$–$V$) characteristics of the studied photodetector illuminated by light at different power densities. (b) Energy band diagrams of the Au/$CsPbBr_3$/Au structure showing the generation, transfer, and collection processes of the photogenerated carriers. (c) Logarithmic plot of the photocurrent versus illumination power. The curve is well fitted using a power law. (d) Photoresponsivity (blck), specific detectivity (red), and EQE (blue) of the photodetectors versus the illuminated light irradiance.[41]

Further improvements in the detector performance of thin-film systems are limited by many factors, such as the large grain boundaries in polycrystalline structures and the low EQE due to the short lifetime of the photogenerated carriers. Therefore, the research focus has shifted toward nano- and micro-structures of perovskites, which are fabricated with fewer grain boundaries, lower defect/trap density, smaller recombination rate, and longer lifetime of the photogenerated carriers compared with thin films.[45,46,55,67–73] Tang *et al.* demonstrated an MSM photodetector based on $CsPb(Br/I)_3$ nanorods. The device was fabricated by placing toluene-dissolved nanorods in a gold interdigital electrode on a $SiO_2$ substrate with 3-μm spacing between adjacent fingers. Under the employed light source (a continuous-wave laser with an excitation wavelength of 532 nm and an optical power of 20 mW), the photosensitivity of the device reached $10^3$; the rise and decay times were 0.68 s and 0.66 s, respectively.[68] Li *et al.* successfully developed high-quality horizontal $CsPbCl_3$ microwire networks with controlled morphology using simple vapor-phase epitaxial growth on mica substrates. This method overcomes the low-solubility problem of CsCl in common solvents. As the evaporation temperature of the source powders increased, the microwire networks thickened and gradually formed a network structure, leading to full film coverage. Well-connected $CsPbCl_3$ microwire networks have also been fabricated as the light absorber in MSM-type perovskite photodetectors (Fig. 7(a)). The photodetectors exhibited a high on/off photocurrent ratio of $2.0 \times 10^3$, a responsivity of 14.3 mA/W, and a fast response speed of 3.212/2.511 ms. More importantly, even the non-encapsulated photodetectors were stable against oxygen and water degradation when operated in continuous-current mode. Long-term operational stability is a challenge in perovskite-based optoelectronic devices, particularly in hybrid halide perovskites, which are vulnerable to environmental heat and oxygen/moisture exposure. All-inorganic perovskites are rendered more stable by replacing methylammonium with inorganic cesium.[26,67,74,75] Real-time photodetectors must operate outdoors under inconsistent conditions, such as harsh, hot environments. Therefore, the temperature tolerance of the photodetectors must be assessed in temperature-dependent photocurrent measurements. The photodetectors efficiently sustained their photodetection ability at a high temperature (373 K) over 9 h of continuous operation, which is ideal for practical applications (Fig. 7(b)). Therefore, inorganic $CsPbCl_3$ microwire networks are expected to be used as the building blocks of high-performance photodetectors that can operate well at high temperatures. The high-temperature operation behaviors of perovskite photodetectors is first reported herein. These results might therefore promote the development of stable and high-efficiency perovskite photodetectors with practical applicability under harsh conditions.[69]

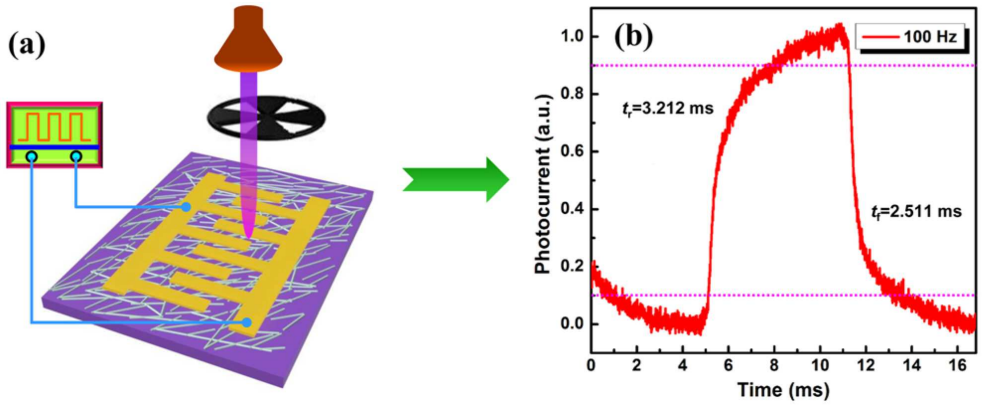



**Fig. 7.** (a) Schematic of the photodetector based on $CsPbCl_3$ microwire networks. (b) Normalized photocurrent of the non-encapsulated $CsPbCl_3$ microwire-network photodetectors over time. The operation continued for 9 h at 373 K.[69]

Zhang *et al.* fabricated ultraviolet photodetectors based on cubic $CsPbCl_3$ nanocrystals. The configuration was a typical indium tin oxide (ITO)/$CsPbCl_3$ nanocrytals/quartz stack. First, a 100-nm-thick $CsPbCl_3$ nanocrystal film was fabricated via spin coating. Next, a pair of interdigitated ITO electrodes (100-nm thick) was thermally evaporated onto the films using a shadow mask, forming a 200-nm-wide and 5-μm-long channel. $CsPbCl_3$ has a relatively large bandgap; therefore, the as-fabricated photodetectors were almost transparent in the visible region. The visible light transmittance was $\sim 90\%$, and ultraviolet light was strongly absorbed in the 300–410-nm region. The device achieved a large on/off photocurrent ratio of $\sim 10^3$ and a photoresponsivity of 1.89 A/W. The rise and decay times of the device were $< 41$ and 43 ms, respectively.[45]

Photodetectors based on single-perovskite single crystals have also been prepared. After determining the appropriate growth conditions, Cha *et al.* fabricated millimeter-sized $CsPbBr_3$ and $Cs_4PbBr_6$ crystals using the anti-solvent vapor-assisted crystallization method in polar solvents at room temperature. Panels (a) and (b) of Fig. 8 display a rectangular orange $CsPbBr_3$ crystal with dimensions of $(0.67 \times 2.0 \times 0.51)$ $mm^3$ and a parallelepiped green $Cs_4PbBr_6$ crystal with dimensions of $(0.56 \times 0.39 \times 0.32)$ $mm^3$, respectively; these samples were the largest crystals grown in solution. The precursor stoichiometry and growth time play important roles in the synthesis of single crystals. The $CsPbBr_3$ crystal was obtained from $PbBr_2$-rich precursor solution in three days, and the $Cs_4PbBr_6$ crystal was crystallized from HBr-added CsBr-rich precursor solution for four days. The responsivity of the single-crystal $CsPbBr_3$ was 2.1 A/W, and the rise and fall times were determined as 0.3 and 5 s, respectively.[70]

The aforementioned results typify the characteristics of an MSM photodetector, namely large photocurrent, high responsivity, and slow response time. Therefore, many researchers have sought ways to improve the performance of photodetectors. For instance, Song *et al.* fabricated two-dimensional (2D) nanosheets of $CsPbBr_3$ and incorporated them into a high-performance photodetector. The structure of this device is presented in Fig. 9(a). The product was pure and uniform (Fig. 9(b)), exhibiting none of the by-products (such as nanometer-sized cubes) that are commonly observed in short-time, hot-injection reactions. A flexible photoconductive detector based on the 2D all-inorganic perovskite $CsPbBr_3$ nanosheets exhibited a high performance (Fig. 9(c)). When irradiated by a light source, electron–hole pairs were generated in the perovskites due to the photoelectric effect (inset of Fig. 9(c)). These electron–hole pairs were rapidly separated and collected by the opposite electrodes under the applied electric field, confirming the effective operation of the $CsPbBr_3$ nanosheet-based photodiode. The conduction band and valence band of the $CsPbBr_3$ nanosheets were obtained via ultraviolet photoelectron spectroscopy and UV–visible absorbance spectroscopy. The photocurrent versus voltage plots obtained under illumination by a 442-nm laser (0.35 $mW/cm^2$) were

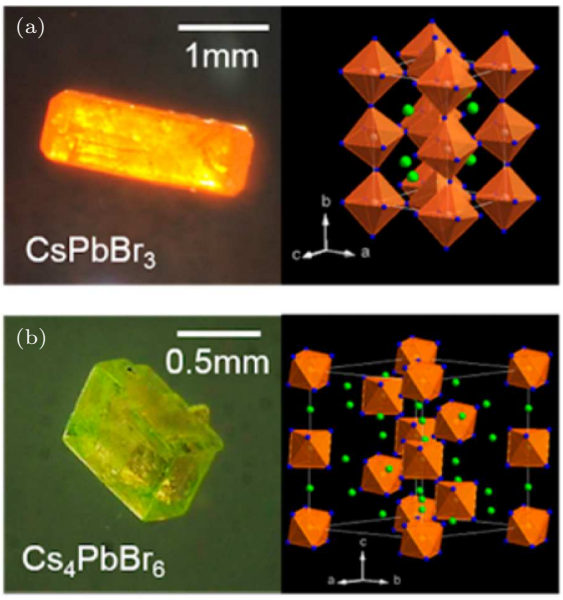



**Fig. 8.** Optical microscopy images and crystal structure diagrams of (a) $CsPbBr_3$ and (b) $Cs_4PbBr_6$ crystals (orange octahedrons, $[PbBr_6]^{4-}$; green dots, Cs atoms; blue dots, Br atoms).[70]

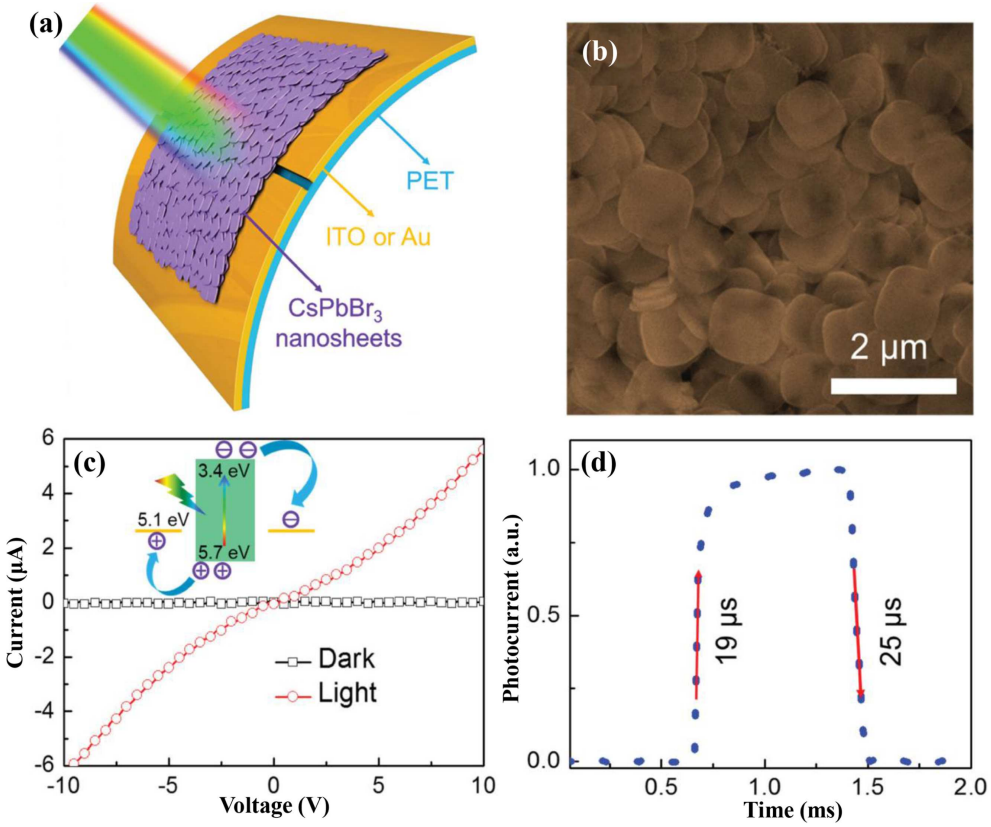



**Fig. 9.** (a) Configuration schematic of the device based on $CsPbBr_3$ nanosheets. (b) High-magnification SEM images of the device. (c) *I–V* characteristics of the photodetector in the dark and under irradiation with 442-nm light (0.35 mW/cm$^2$). Inset: working principle of the photodetector. (d) Normalized high-resolution photoresponse, showing the rise and decay times.[71]

typically linear and symmetrical, indicating that the $CsPbBr_3$ nanosheets were well dispersed on the ITO electrode with good ohmic contact. The as-prepared nanosheets can be well dispersed in various solvents, increasing the opportunities for fabricating solution-based optoelectronic devices. In addition, the 2D $CsPbBr_3$ nanosheets possessed excellent electronic-transport properties. A high photosensitivity (0.64 A/W) and an on/off ratio exceeding $10^4$ were reported in the studied device. The device was remarkably stable, fluctuating by $< 2.6\%$ after 12-h irradiation with the 442-nm laser (10 mW/cm$^2$). By virtue of the high crystal quality and the atomic 2D plane of the $CsPbBr_3$ nanosheets, the response times of the photodetector were very fast ($t_r = 19$ μs, $t_f = 25$ μs (Fig. 9(d)). These results demonstrate the huge application potential of the as-synthesized $CsPbBr_3$ nanosheets in high-sensitivity detectors.[71]

Pang *et al.* demonstrated a $CsPbBr_3$ photodetector based on high-quality, well-aligned nanoribbons, confirming that 6,6-phenyl-C61-butyric acid ethyl ester (PCBM) not only passivates the defects on the $CsPbBr_3$ nanoribbon surface but also transfers the charge. Figure 10(a) presents a schematic and the logarithmic *I–V* curves of the studied photodetectors made of $CsPbBr_3$ nanoribbons. The curves were collected under light illumination and in darkness. The high signal-to-noise ratio ($\sim 10^4$) implies a high sensitivity to incident light. As shown in Fig. 10(b), the photoresponses of the as-fabricated photodetectors are regular rectangular pulses. The hybrid 6,6-phenyl-C 61-butyric acid methyl ester (PCBM)–$CsPbBr_3$ photodetectors shortened the response and recovery times from 13.3 and 7.1 ms (in bare $CsPbBr_3$ photodetectors) to 8.7 and 3.5 ms, respectively. Moreover, the photoresponsivity was enhanced to 18.4 A/W due to the high material integrity of the $CsPbBr_3$ nanoribbons and the efficient interfacial charge transfer from the perovskites to the PCBM passivation layer.[73]

More recently, Tong *et al.* applied dual-phase inorganic perovskites ($CsPbBr_3$–$CsPb_2Br_5$) as the light-harvesting layer in photodetectors. The dual-phase perovskites were synthesized using the physical vapor deposition method on rigid and flexible substrates. More specifically, CsBr and $PbBr_2$ films were sequentially deposited on the substrates via thermal evaporation, controlling the $PbBr_2$ excess by regulating the thickness. The deposition was followed by a post-annealing step in air at 13 °C to form the dual-phase inorganic perovskites. The halogen ions ($Br^-$) were enriched on the surfaces of the inorganic perovskite films, enabling a wide-bandgap semiconductor of $CsPb_2Br_5$ in the film and a consequent self-passivation phenomenon on the interface, which might reduce the charge recombination at the interface. The inset of Fig. 11(a) is a photograph of the $2.5 \times 1.5$-cm$^2$ dual-phase inorganic perovskite film on the glass substrate. The film is quite uniform and

emits green light under ultraviolet illumination. The inorganic perovskites absorb wavelengths shorter than $\sim$ 535 nm, approximately 10 nm lower than the absorption cutoff of pure $CsPbBr_3$ film. The photodetector exhibited a high photoresponsivity (0.375 A/W) and a specific detectivity of $\sim 10^{11}$ Jones, along with fast response times ($t_r \sim 280$ μs; and $t_f \sim 640$ μs, respectively; Fig. 11(b)).[76] These results highlight the great potential of dual-phase inorganic perovskite films in optoelectronic devices, particularly in flexible device applications.

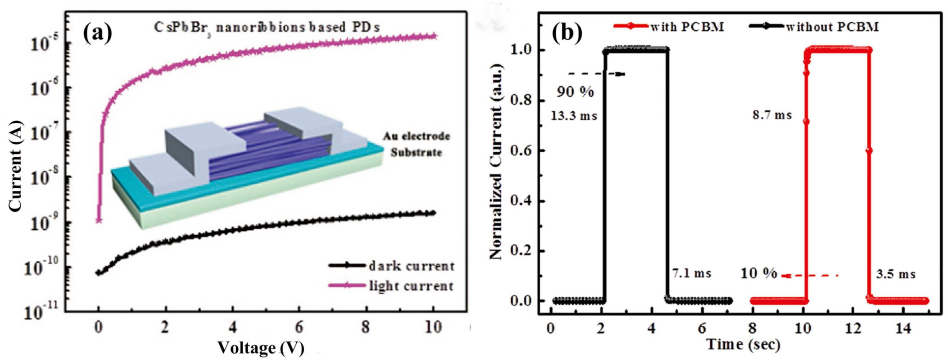



**Fig. 10.** (a) Logarithmic *I–V* curves of the photodetector devices under light illumination (504 nm, 10 mW/cm$^2$) and in darkness. (b) Time-resolved photocurrents in the photodetectors based on bare $CsPbBr_3$ nanoribbon film and in PCBM passivated $CsPbBr_3$ nanoribbon film.[73]

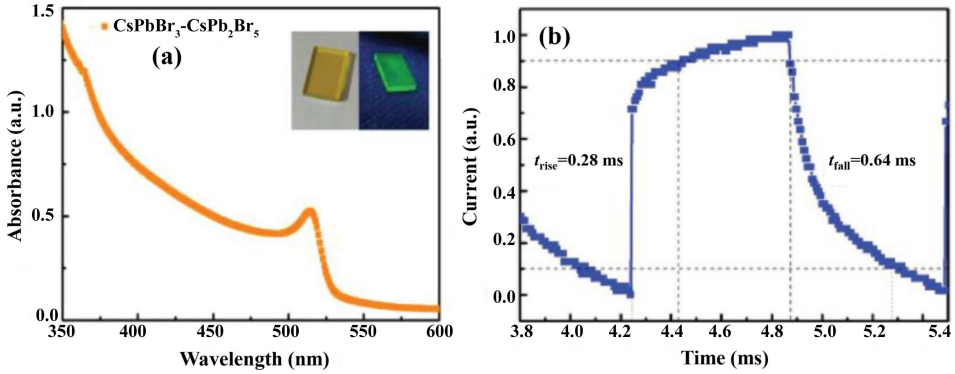



**Fig. 11.** (a) Ultraviolet–visible absorbance spectrum of inorganic dual-phase perovskite film; inset: photographs of the inorganic perovskite film on glass substrate under ambient conditions (left) and under ultraviolet illumination (right). The films are sized 2.5 × 1.5 cm$^2$. (b) Corresponding magnified and normalized plots of one response cycle for estimating the rise and fall times of the photodetector.[76]

### 3.3. Heterojunction photodetectors

The planar MSM structure is the typical architecture of perovskite photodetectors. However, because the device lacks an efficient charge-blocking layer or a built-in field, the dark-noise current is high and the response speed is slow, limiting further improvements of the detection limit. To overcome the drawbacks of the MSM structure, heterojunction photodetectors have been extensively studied. Bao *et al.* processed high-performance heterojunction photodetectors from all-inorganic $CsPbI_xBr_{3-x}$ thin films (Fig. 12(a)). The hole transport, electron transport, and exciton blocking layers were p-type polymer poly[bis(4-phenyl) (2,4,6-trimethylphenyl)amine] (PTAA), small molecular PCBM, and bathocuproine (BCP), respectively. The $CsPbI_xBr_{3-x}$ film was deposited via one-step spin coating. After modifying the substrate with ethoxylated polyethylenimine (PEIE), the crystal quality and surface coverage of the $CsPbI_xBr_{3-x}$ film considerably improved. Panels (b) and (c) of Fig. 12 present the *I–V* curves of the fabricated photodetectors based on the $CsPbIBr_2$ and $CsPbBr_3$ thin films, respectively. The dark currents of the $CsPbIBr_2$ and $CsPbBr_3$ devices under a −0.3-V bias were approximately $6.0 \times 10^{-6}$ and $4.8 \times 10^{-5}$ mA/cm$^2$, respectively. Moreover, the approximate detectable limit and response time of the resulting $CsPbIBr_2$ photodetectors were 21.5 pW/cm$^2$ and 20 ns, respectively. This confirms that the device can follow a quickly varying optical signal and suggests the great potential of such heterostructured photodetectors in optical communication.[77]

Lu *et al.* recently proposed a new hybrid 3D architecture that integrates inorganic perovskite QDs with high quantum yield on hydrogenated amorphous silicon (a-Si:H) radial junctions (RJs) constructed over silicon nanowires (SiNWs). This architecture demonstrated an ultrafast and efficient optoelectronic down-conversion for solar-blind ultraviolet detection. Figure 13(a) schematizes the multilayered a-Si thin film with the PIN RJ structure constructed around SiNW cores. The film was grown using a plasma-enhanced chemical vapor deposition method involving a vapor–liquid–solid growth mechanism catalyzed by tin nanoparticles. For photodetection appli-

cations, the colloidal CsPb$X_3$ QDs were uniformly spin coated on the SiNWs. These high-quality CsPb$X_3$ QDs with a tunable bandgap over the entire visible region were successfully integrated in the photonic a-Si:H RJs. The strong light trapping, absorption, and excitation effects combined in the device, realizing an ultrafast solar-blind ultraviolet response with rise/fall response time scales of 0.48/1.03 ms and a high responsivity (54 mA/W at 200 nm or 32 mA/W at 270 nm; Fig. 13(b)). Moreover, the device requires no external power supply. These successes pave the way toward large-area manufacturing of high-performance ultraviolet detectors based on Si-based perovskites using a scalable and low-cost procedure.[78]

Zhou *et al.* fabricated self-powered all-inorganic $CsPbBr_3$ perovskites for microcrystal photodetectors with high detectivity and a fast response time. Threrein, $CsPbBr_3$ perovskite microcrystals were prepared directly on $SnO_2$-coated substrates using a modified inverse temperature crystallization method. The resulting microcrystals were $\sim$ 10 μm in size and $\sim$ 11 μm in thickness (single layer). Encouraged by the low trap-state density, self-powered thin-film photodetectors were fabricated based on the $CsPbBr_3$ microcrystals. Figure 14(a) presents a band diagram of the $CsPbBr_3$ microcrystal thin-film photodetectors (with a structure of glass/ITO/$SnO_2$/perovskite microcrystal/spiro-OMeTAD/Au). In this structure, the $SnO_2$ and spiro-OMeTAD are the electron- and hole-selective layers, respectively. When illuminated with a 473-nm laser (100 mW), the responsivity, detectivity, on/off ratio, and LDR of the $CsPbBr_3$ microcrystal photodetectors were 0.172 A/W, $4.8 \times 10^{12}$ Jones, $1.3 \times 10^5$, and up to 113 dB, respectively. The rise and fall times were observed as $\sim$ 0.14 and 0.12 ms, respectively, at a light modulation frequency of 500 Hz (Fig. 14(b)). These performances significantly improved over those of photodetectors based on polycrystalline perovskite thin films and were comparable with those of photodetectors based on single-crystal perovskites.[79]

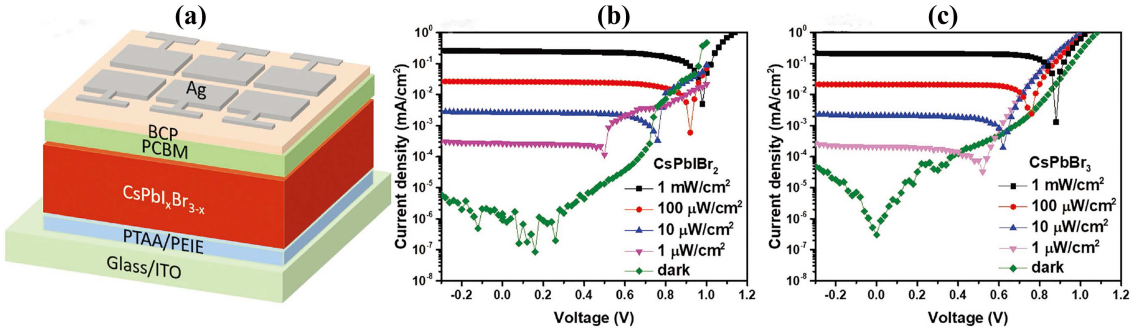



**Fig. 12.** (a) Schematic of the structure of the photodetector based on all-inorganic perovskites $CsPbI_xBr_{3-x}$. (b, c) *I*–*V* curves of the $CsPbIBr_2$- and $CsPbBr_3$-based photodetectors in the dark and under illumination with 450-nm monochromatic light of different intensities (1 μm/cm$^2$ to 1 mW/cm$^2$).[77]

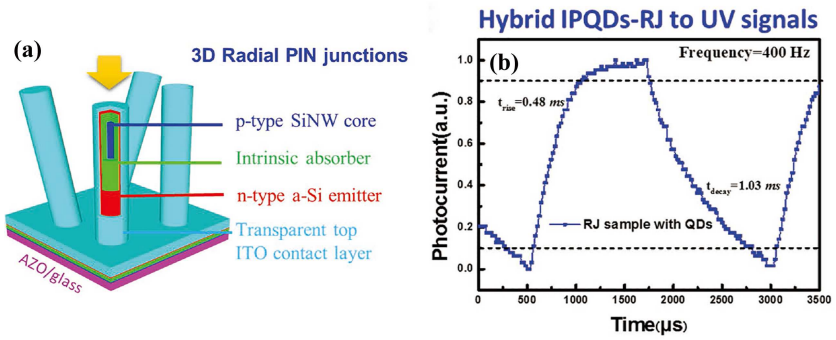



**Fig. 13.** (a) Schematic of the multilayered a-Si thin-film PIN RJ structure constructed on SiNWs. (b) Magnified and normalized plots of one response cycle showing the rise and fall times.[78]

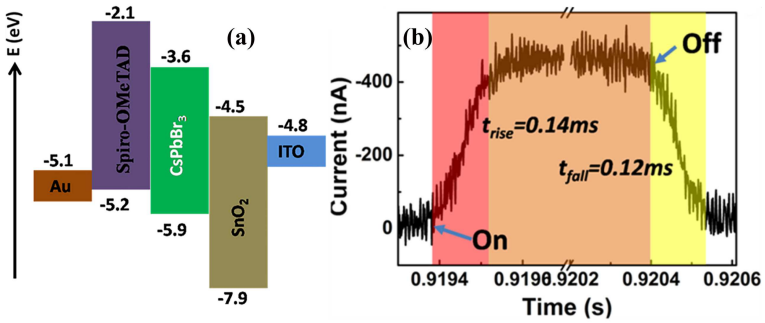



**Fig. 14.** (a) Energy band diagram of the $CsPbBr_3$ microcrystal perovskite photodetector. (b) Rising and falling edges for estimating rise and fall times of the photodetector at 500 Hz.[79]

Song *et al.* proposed a novel photodetector structure based on a ZnO hollow ball/$CsPbBr_3$ heterojunction. The ZnO hollow balls function as an ultraviolet response center, and the $CsPbBr_3$ is designed as a green light-emitting material. The $CsPbBr_3$ perovskites shield the ZnO from air contact and allow the smooth passage of the photogenerated holes to GaN. Owing to the superior ultraviolet-light trapping characteristics of the device, the ultraviolet light response is huge, with an on/off ratio and specific detectivity of 16527 and $2.4 \times 10^{13}$ Jones, respectively. Similar to Lu *et al.*'s device,[26] the proposed photodetector operates accurately without requiring an external power supply. The $CsPbBr_3$ insertion improved the dual-functional performance from that of the traditional ZnO/GaN structure at various wavelengths. This improvement was conferred by the better contact interface and the green-light emission center. The ZnO/$CsPbBr_3$/GaN structure yielded much higher values than the ZnO/GaN structure, and its response region was widened to 550 nm, except in the ultraviolet region. Additionally, the ZnO/$CsPbBr_3$/GaN structure displayed a blue electroluminescence under a low-threshold voltage. By separating the light-responsive and actively emitting regions, this structure avoids the contradictory principles of carrier transport, possibly enabling high-performance dual-functional devices.[80]

## 4. Lead-free halide perovskite photodetectors

Despite the remarkable progress of high-performance perovskite photodetectors constructed from lead–halide absorbers $APbX_3$, the toxicity of lead remains a concern in the large-scale applications of these photodetectors. Substituting lead (Pb) with bivalent tin (Sn) might resolve the toxicity problem. Recently, $CsSnX_3$ perovskite ($X$ = Cl, $Cl_{0.5}Br_{0.5}$, Br, $Br_{0.5}I_{0.5}$, and I)[81,82] and $Cs_2SnI_6$ perovskite derivatives have been synthesized via a facile hot-injection process.[83] However, most of these materials are used in light-emitting diodes, laser, and solar cells.[84–90] Photodetector applications of lead-free halide perovskites, particularly all-inorganic Sn-based perovskites, are scarce. Sb-based perovskites are another promising alternative. $Cs_3Sb_2X_9$ ($X$ = Cl, Br, and I) QDs have been fabricated via solution-phase synthesis and applied in luminescent devices and solar cells.[91–94] Pradhan *et al.* synthesized $Cs_3Sb_2Cl_9$ nanocrystals by employing a colloidal synthesis route. Guided by their experimental observations, they modeled the atomic arrangements of the trigonal and orthorhombic phases in the nanowires. In both phases, the Cs and Cl atoms showed a close-packed arrangement with the Sb atoms (Figs. 15(a) and 15(b)). Uniform nanowires with lengths of several microns and different aspect ratios were obtained by tuning the precursors and ligands. Furthermore, photodetectors based on $Cs_3Sb_2Cl_9$ nanowires were fabricated on pre-patterned gold electrodes with a channel length of 100 nm (Fig. 15(c)). The $I$–$V$ characteristics showed semiconducting behavior under both dark and illuminated conditions (Fig. 15(d)); however, illumination considerably enhanced the current. A highly sensitive photodetecting response, with no photocurrent decay, was observed over repetitive on/off illumination cycles (Fig. 15(e)). The rise and decay times of the photodetectors were 0.13 and 0.23 s, respectively, at a bias voltage of 0.9 V (Fig. 15(f)). The fast photoresponsive properties of perovskite nanocrystals make them prospective materials for optoelectronic applications. Herein, an approach for fabricating environmental friendly analogous $Cs_3Sb_2X_9$ ($X$ = Br, I) perovskite nanocrystals with high material stability is proposed. This new material system is potentially applicable to other optoelectronic devices, such as memory and solar cells.[95]

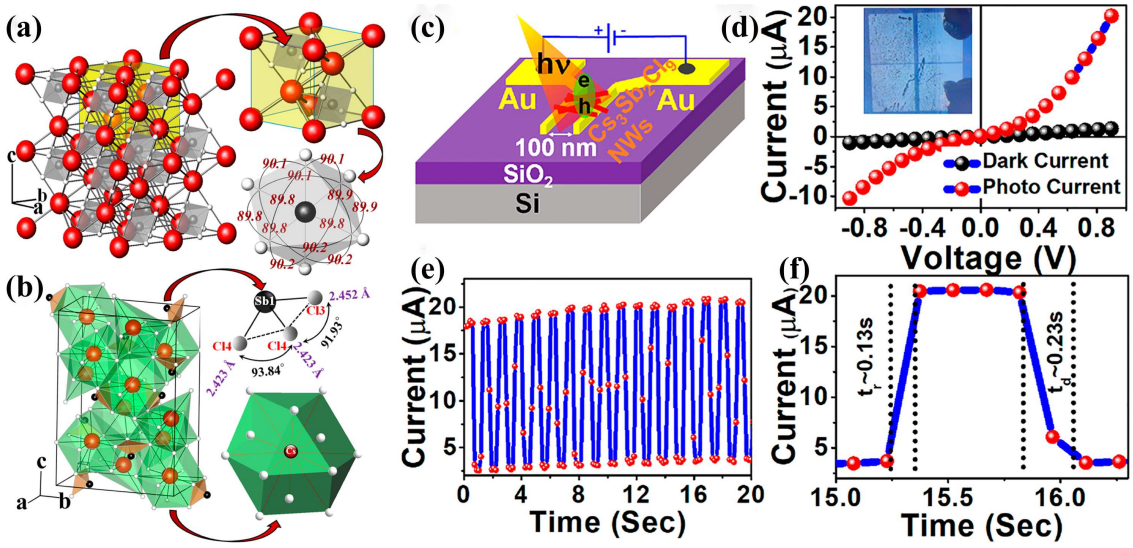



**Fig. 15.** (a) Atomic arrangements of the trigonal phase of $Cs_3Sb_2Cl_9$ nanowires: unit cell (top) and $SbCl_6$ octahedra (bottom). (b) Atomic arrangements of the orthorhombic phase: irregular triangular planar geometry of Sb and Cl (top) and polyhedron (bottom). Black, red, and white spheres correspond to Sb, Cs, and Cl, respectively. (c) Schematic of the photodetector device. (d) Current versus voltage characteristics of the $Cs_3Sb_2Cl_9$ nanowires under dark and light-illuminated conditions. Inset is an optical image of the device. (e) Photo-switching behavior at 0.9 V, revealing fast on/off switching states with a time interval of 500 ms. (f) Rise and decay times of a single on/off cycle.[95]

All-inorganic Bi-based perovskites have also been successfully synthesized.[96–102] Tong *et al.* developed a sensitive red-light photodetector based on $CsBi_3I_{10}$ perovskite thin films fabricated via spin coating. In an optoelectronic study, the as-assembled device demonstrated obvious sensitivity to red-light illumination, excellent reproducibility, and good spectral selectivity. Figure 16 schematizes the stepwise fabrication process of the $CsBi_3I_{10}$ perovskite film-based photodetector. The $CsBi_3I_{10}$ perovskite film was fabricated by directly spin coating the precursor on glass. After synthesis, the brownish-black, inorganic, lead-free perovskite film and two metal electrodes (Au: 50 nm) were deposited using a shadow mask. The as-assembled device was then placed on a printed circuit board (PCB). To stabilize the device, the two Ti/Au electrodes were connected to the PCB using aluminum wires (5 μm), which were secured via wire bonding. The as-fabricated perovskite device exhibited high sensitivity to red light, with excellent reproducibility, good spectral selectivity, and a high on/off ratio ($10^5$). Under 650-nm illumination, the responsivity and specific detectivity of the device were estimated as 21.8 A/W and $1.93 \times 10^{13}$ Jones, respectively. Moreover, the perovskite photodetector detected pulsed light at high frequency (3000 Hz). The rise and fall times were estimated as 0.33 and 0.38 ms, respectively. These excellent device parameters, coupled with the strong device stability under ambient conditions, corroborate the promising prospect of this $CsBi_3I_{10}$-perovskite-based photodetector in future optoelectronic device applications.[43]

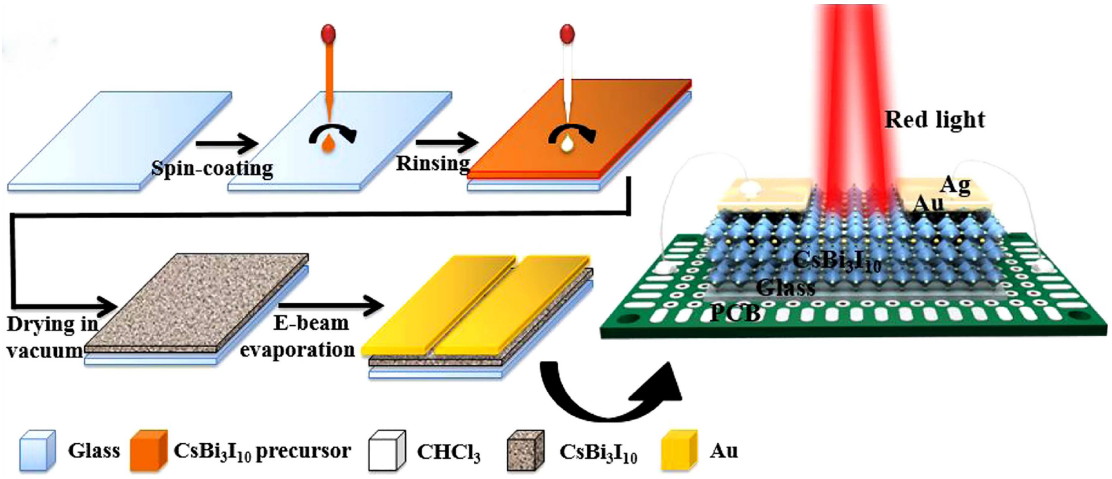



**Fig. 16.** Stepwise fabrication process of the $CsBi_3I_{10}$ perovskite film-based photodetector.[43]

The heterovalent substitution concept, in which a pair of Pb(II) ions is replaced by a monovalent $B^+$ and a trivalent $B^{3+}$ ion to form an $A_2B^+B^{3+}X_6$ double-perovskite structure, has also attracted considerable attention. $Cs_2AgBiBr_6$ is regarded as a highly promising replacement of conventional lead halides.[102–104] Lei *et al.* fabricated lead-free perovskite photodetectors with the light absorbers of double-perovskite $Cs_2AgBiBr_6$ thin film synthesized using the one-step spin coating. The reaction sources were high-purity CsBr, AgBr, and $BiBr_3$. To investigate the potential applications of such $Cs_2AgBiBr_6$ thin films in photoelectric response, Lei *et al.* constructed a photoconductive detector with a coplanar MSM interdigitated patterned Au-electrode configuration. Figure 17(a) presents the energy band diagram of the Au/$Cs_2AgBiBr_6$/Au structure, showing the generation, transfer, and collection processes of the photogenerated carriers. Figure 17(b) displays the spectral response of the photodetector within 300–800 nm. The responsivity was maximized at ~ 510 nm. Increasing the wavelength from 510 to 900 nm, or decreasing it from 510 to 300 nm, elicited a sharp reduction in the device sensitivity. Figure 17(c) depicts the *I*–*V* characteristics of the device under dark and light-illuminated conditions. As the illumination power increased from 0 to 13.63 mW, the device photocurrent gradually increased because the number of photogenerated carriers is proportional to the absorbed photon flux. Moreover, the dependence of the photocurrent on the light illumination power was well fitted by a power law $I = mP^{\mu}$, where $m$ is the proportionality constant for a given wavelength, $P$ represents the illumination power of the illuminating light, and $\mu$ determines the response of the photocurrent to the light intensity. The data were best described by a sublinear behavior with $\mu = 0.76$ (Fig. 17(d)). Figure 17(e) plots the photodetector responsivity, and figure 17(f) plots the specific detectivity and EQE, as functions of incident light power. The responsivity, on/off photocurrent ratio, specific detectivity, and EQE were determined as 7.01 A/W, $2.16 \times 10^4$, $5.66 \times 10^{11}$ Jones, and 2146%, respectively. From the photocurrent response profile recorded at 50 and 500 Hz, the rise and fall times of the $Cs_2AgBiBr_6$ thin-film photodetector were estimated as 5.77 and 5.97 ms, respectively, at 50 Hz and 956 and 995 μs, respectively, at 500 Hz.[105]

Recently, Wu *et al.* reported a self-powered photodetector based on the ITO/$SnO_2$/$Cs_2AgBiBr_6$/Au structure but without a hole-transport layer. The device is self-powered with two

responsivity peaks at 350 and 435 nm, suitable for light detection within 320–400 nm and deep-blue light, respectively. Owing to the high integrity of $Cs_2AgBiBr_6$ thin film and the efficient interface charge transfer from perovskite to the underlying $SnO_2$, the photodetector demonstrated a high responsivity of 0.11 A/W at 350 nm and a quick response time of $< 3$ ms, which is considerably higher than those of other semiconductor oxide heterojunction-based ultraviolet detectors. With its non-toxic and stable double-perovskite active layer, this device is very promising for practical applications.[106]

Table 1 compares the responsivities, specific detectivities, on/off ratios, and response times of the all-inorganic halide perovskite photodetectors. The device performances, particularly the photoresponse times, vary considerably among the structures. The rise/fall response times reported in Refs. [70] and [71] are 0.3/5.0 s and 19/25 μs, respectively. Accordingly, many possible factors, including photocarrier generation and separation, carrier transport, carrier collection, and resistance–capacitance of the system, should be considered.[107] The photocarrier generation and separation process largely depend on the device structure. For example, photovoltaic detectors possess a built-in electric field that accelerates the photocarrier generation and separation processes, facilitating spatial separation and the transfer of photogenerated carriers. This behavior, which enables operation at zero bias, does not occur in the MSM structured device. The carrier-transport process strongly depends on the microstructure characteristics of the perovskite absorber layer. When perovskite polycrystalline films are employed as the light absorber in photodetectors, the photogenerated carriers can be trapped by defect states in the interfacial areas among the nanocrystallites and the photoresponse is slowed. In contrast, perovskite micro/nanocrystalline structures are characterized by few grain boundaries, long lifetime, low defect/trap density, and small recombination rate. These properties favor a fast photoresponse and high photoresponsivity. The carrier collection process critically depends on the electrode distance and the semiconductor–metal contact behavior. The resistance–capacitance determines the test limit of the studied photodetectors. This performance measure also varies widely among thus-reported studies.

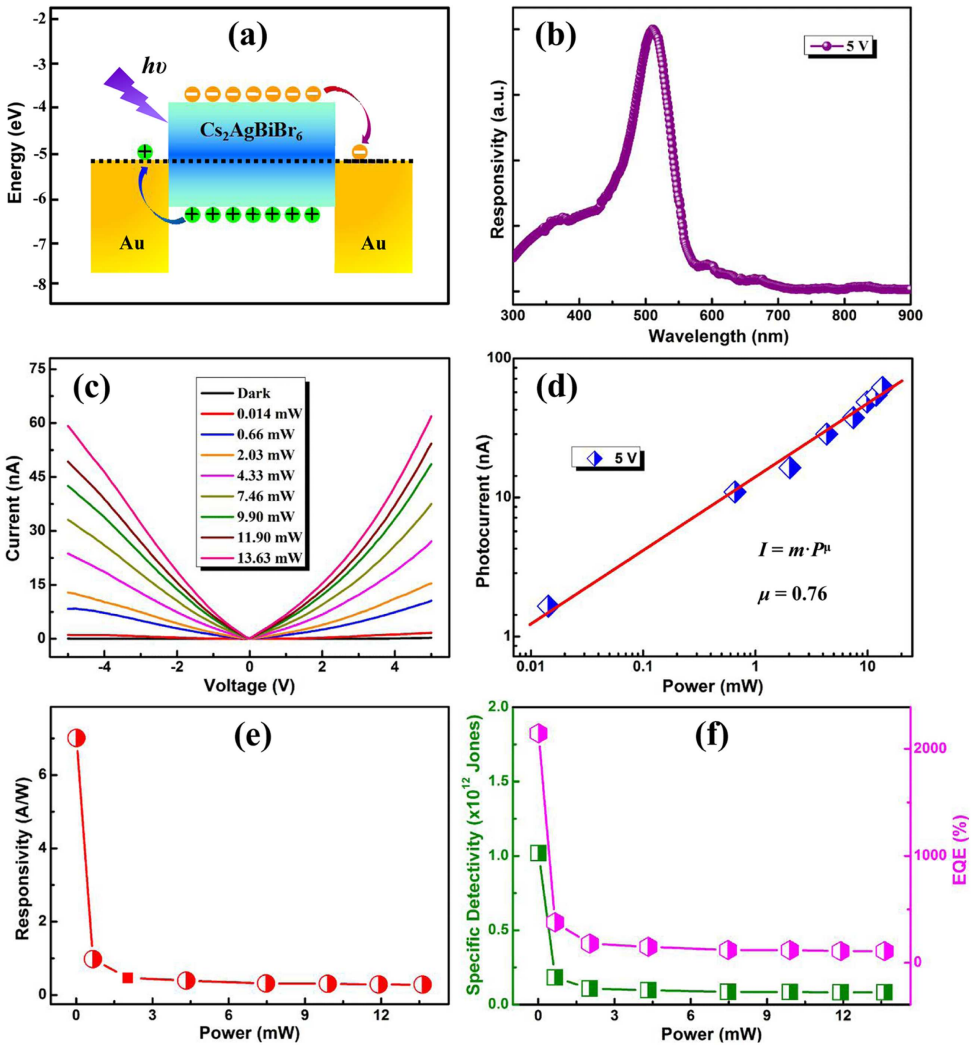



**Fig. 17.** (a) Energy band diagram of the Au/$Cs_2AgBiBr_6$/Au structure, showing the generation, transfer, and collection processes of the photogenerated carriers. (b) Spectral responses of the $Cs_2AgBiBr_6$ thin-film photodetector. (c) *I*–*V* curves of the photodetector under light with different illumination powers. (d) Logarithmic plot of photocurrent versus illumination power. (e) Photoresponsivity and (f) specific detectivity and EQE of the photodetector versus light illumination power.[105]

**Table 1.** Summary of all-inorganic perovskite-based photodetectors.

| Device structure | Material structure | Responsivity/(A/W) | $D^*/10^8$ Jones | On/off ratio | Response time/ms | Ref. |
|---|---|---|---|---|---|---|
| Ti–Au/Graphene–$CsPbBr_{3-x}I_x$/Ti–Au | nanocrystals | $8.2\times10^8$ | $2.4\times10^8$ | – | 810/3650 | [25] |
| Au/$CsPbBr_3$/Au | thin films | 55 | – | $10^5$ | 0.43/0.318 | [41] |
| Au/$CsPbBr_3$-ZnO/Au | thin films | 4.25 | – | $10^4$ | 0.21/0.24 | [42] |
| Au/$Cs_3Bi_2I_9$/Au | thin films | 21.8 | $1.93\times10^5$ | $10^5$ | 0.33/0.38 | [43] |
| ITO/$CsPbCl_3$/ITO | nanocrystals | 1.89 | – | $10^3$ | 41/43 | [45] |
| Au/$CsPbBr_3$/Au | nanoplatelets | 34 | $7.5\times10^4$ | – | 0.6/0.9 | [46] |
| Au/$CsPbBr_3$/Au | nanoworks | – | – | $10^3$ | 100/100 | [55] |
| Au/$CsPbBr_3$–Au NCs/Au | nanoparticles | 0.01 | 4.56 | $10^6$ | 0.2/1.2 | [67] |
| Au/$CsPb(Br/I)_3$/Au | nanorods | – | – | $10^3$ | 680/660 | [68] |
| Ag/$CsPbCl_3$/Ag | microwire | 0.0143 | – | $2\times10^3$ | 3.212/2.511 | [69] |
| Au/$CsPbBr_3$/Au | single crystal | 2.1 | – | – | 300/5000 | [70] |
| Au or ITO/2D $CsPbBr_3$/Au or ITO | nanosheets | 0.64 | – | $10^4$ | 0.019/0.025 | [71] |
| ITO/CsPbBr3/ITO | microcrystals | 60000 | $10^5$ | – | 0.5/1.6 | [72] |
| Au/$CsPbBr_3$/Au | nanoribbons | 18.4 | $6.1\times10^4$ | 8616 | 8.7/3.5 | [73] |
| Au/$CsPbBr_3$/Au | nanosheets | – | – | $10^2$ | 17.8/14.7 | [75] |
| Ti–Au/$CsPbBr_3$–$CsPb_2Br_5$/Ti–Au | thin films | 0.375 | 2960 | 380 | 0.28/0.64 | [76] |
| PTAA/PEIE/$CsPbIBr_2$/PCBM/BCP | thin films | 0.28 | $9.7\times10^4$ | – | $2\times10^{-5}$ | [77] |
| $CsPbX_3$/$\alpha$-Si radial junction | quantum dots | 0.054 | – | $2.1\times10^3$ | 0.48/1.03 | [78] |
| Au/spiro-OMeTAD/$CsPbBr_3$/$SnO_2$/ITO | microcrystals | 0.172 | $4.8\times10^4$ | $1.3\times10^5$ | 0.14/0.12 | [79] |
| FTO/ZnO/$CsPbBr_3$/GaN/In | thin films | 0.23 | $2.4\times10^5$ | $10^4$ | 281/104 | [80] |
| Au/$Cs_3Sb_2Cl_9$/Au | nanowires | 3616 | 0.0125 | – | 130/230 | [95] |
| Au/$Cs_2AgBiBr_6$/Au | thin films | 7.01 | 5660 | $2.2\times10^4$ | 0.956/0.995 | [105] |
| ITO/$SnO_2$/$Cs_2AgBiBr_6$/Au | thin films | 0.11 | 240 | – | 3/2 | [106] |
| Au/$CsPbBr_3$/Au | microparticles | 0.18 | – | $8\times10^3$ | 1.8/1.0 | [108] |
| graphite/$CsPbBr_3$/graphite | microcrystals | 2.1 | – | $10^3$ | 0.25/0.45 | [109] |
| Au/$CsPbI_3$/Au | nanocrystals | – | – | $10^5$ | 24/29 | [110] |
| Al/$CsPbI_3$/ITO | nanowires | 0.0067 | 1.57 | – | 292/234 | [111] |
| Au/$CsPbBr_3$/Au | single crystal | 2 | – | $10^3$ | 0.111/0.575 | [112] |
| Ag/$CsPbBr_3$–CNTs/Ag | nanosheets | 31.1 | – | 832 | 0.016/0.38 | [113] |
| ITO/$CsPbBr_3$–ZnO NPs/Ag | films | 0.0115 | – | 12.86 | 409/17.92 | [114] |
| Au/$\alpha$ –$CsPbI_3$-$NaYF_4$:Yb,Er QDs/Au | quantum dots | 1.5 | – | $10^4$ | 5/5 | [115] |
| Au/$MoS_2$–$CsPbBr_3$/Au | nanosheets | 4.4 | 250 | $10^4$ | 0.72/1.01 | [116] |

## 5. Conclusions

Owing to the unprecedented optoelectronic properties of halide perovskite-based solar cells, perovskite photodetectors have considerably progressed over the past few years. This study has comprehensively overviewed the recent advances in all-inorganic halide perovskite materials and photodetectors with different device structures, including lead-based and lead-free halide perovskites. Recent reports on lead-free perovskite photodetectors were also discussed. The reported environmentally friendly alternatives are desired in practical applications. However, many unsolved problems remain and the stability and performance of halide perovskite-based devices require further development. It is hoped that this study will promote research on all-inorganic perovskite photodetectors, securing their practical applicability in the foreseeable future.

## References


[1] Lee M M, Teuscher J, Miyasaka T, Murakami T N and Snaith H J 2012 *Science* **338** 643

[2] Baeg K J, Binda M, Natali D, Caironi M and Noh Y Y 2013 *Adv. Mater.* **25** 4267

[3] Koppens F H L, Mueller T, Avouris P, Ferrari A C, Vitiello M S and Polini M 2014 *Nat. Nanotechnol.* **9** 780

[4] Dong Q F, Fang Y J, Shao Y C, Mulligan P, Qiu J, Cao L and Huang J S 2015 *Science* **347** 967

[5] Li Y, Shi Z F, Lei L Z, Zhang F, Ma Z Z, Wu D, Xu T T, Tian Y T, Zhang Y T, Du G T, Shan C X and Li X J 2018 *Chem. Mater.* **30** 6744

[6] Guo Y L, Liu C, Tanaka H and Nakamura E 2015 *J. Phys. Chem. Lett.* **6** 535

[7] Saidaminov M I, Adinolfi V, Comin R, Abdelhady A L, Peng W, Dursun I, Yuan M, Hoogl, S, Sargent E H and Bakr O M 2015 *Nat. Commun.* **6** 8724

[8] Adinolfi V, Ouellette O, Saidaminov M I, Walters G, Abdelhady A L, Bakr O M and Sargent E H 2016 *Adv. Mater.* **28** 7264

[9] Deng W, Zhang X J, Huang L M, Xu X Z, Wang L, Wang J C, Shang Q X, Lee S T and Jie J S 2016 *Adv. Mater.* **28** 2201

[10] Shi Z F, Sun X G, Wu D, Xu T T, Zhuang S W, Tian Y T, Li X J and Du G T 2016 *Nanoscale* **8** 10035

[11] Zheng Z, Zhuge F W, Wang Y G, Zhang J B, Gan L, Zhou X, Li H Q and Zhai T Y 2017 *Adv. Funct. Mater.* **27** 1703115

[12] Shi Z F, Li Y, Zhang Y T, Chen Y S, Li X J, Wu D, Xu T T, Shan C X and Du G T 2017 *Nano Lett.* **17** 313

[13] Zhang Z X, Zeng L H, Tong X W, Gao Y, Xie C, Tsang Y H, Luo L B and Wu Y C 2018 *J. Phys. Chem. Lett.* **9** 1185

[14] Liu Y C, Zhang Y X, Zhao K, Yang Z, Feng J S, Zhang X, Wang K, Meng L, Ye H C, Liu M and Liu S Z 2018 *Adv. Mater.* **30** 1707314

[15] Hu W, Wu R S, Yang S Z, Fan P, Yang J L and Pan A L 2017 *J. Phys. D: Appl. Phys.* **50** 375101

[16] Hu W, Huang W, Yang S Z, Wang X, Jiang Z Y, Zhu X L, Zhou H, Liu H J, Zhang Q L, Zhuang X J, Yang J L, Kim D H and Pan A L 2017 *Adv. Mater.* **29** 1703256

[17] Stranks S D, Eperon G E, Grancini G, Menelaou C, Alcocer M J P, Leijtens T, Herz L M, Petrozza A and Snaith H J 2013 *Science* **342** 341

[18] Zhang F, Shi Z, Ma Z, Li Y, Li S, Wu D, Xu T, Li X, Shan C and Du G 2018 *Nanoscale* **10** 20131

[19] Jiang M, Deng N H, Wang L, Xie H M and Qiu Y Q 2018 *Chin. Phys. B* **27** 067102

[20] Huang H M, Jiang Z Y and Luo S J 2017 *Chin. Phys. B* **26** 096301

[21] Zhang Y Y, Chen S Y, Xu P, Xiang H J, Gong X G, Walsh A and Wei S H 2018 *Chin. Phys. Lett.* **35** 036104

[22] Kwak D H, Lim D H, Ra H S, Ramasamy P and Lee J S 2016 *RSC Adv.* **6** 65252

[23] Echtermeyer T, Britnell L, Jasnos P, Lombardo A, Gorbachev R, Grigorenko A, Geim A, Ferrari A and Novoselov K 2011 *Nat. Commun.* **2** 458

[24] Liu Y, Cheng R, Liao L, Zhou H, Bai J, Liu G, Liu L, Huang Y and Duan X 2011 *Nat. Commun.* **2** 579

[25] Furchi M, Urich A, Pospischil A, Lilley G, Unterrainer K, Detz H, Klang P, Andrews A M, Schrenk W and Strasser G 2012 *Nano Lett.* **12** 2773

[26] Protesescu L, Yakunin S, Bodnarchuk M I, Krieg F, Caputo R, Hendon C H, Tang R X, Walsh A and Kovalenko M V 2015 *Nano Lett.* **15** 3692

[27] Song J Z, Li J, Li X M, Xu L, Dong Y and iB H 2015 *Adv. Mater.* **27** 7162

[28] Shi Z F, Li Y, Li S, Li X J, Wu D, Xu T T, Tian Y T, Chen Y S, Zhang Y T, Zhang B L, Shan C X and Du G T 2018 *Adv. Funct. Mater.* **28** 1707031

[29] Dong Y H, Zou Y S, Song J Z, Song X F and Zeng H B 2017 *J. Mater. Chem. C* **5** 11369

[30] Wang X G, Li M M, Zhang B, Wang H, Zhao Y and Wang B H 2018 *Organic Electron.* **52** 172

[31] Wang H and Kim D H 2017 *Chem. Soc. Rev.* **46** 5204

[32] Wang P H, Gong C H, Rao G F, Hu K, Wang X P, Yan C Y, Dai L P, Wu C Y and Xiong J 2018 *Adv. Opt. Mater.* **6** 1701302

[33] Li S G, Zhang C, Song J J, Xie X H, Meng J Q and Xu S J 2018 *Crystals* **8** 220

[34] Ahmadi M, Wu T and Hu B 2017 *Adv. Mater.* **29** 1605242

[35] Chen S and Shi G Q 2017 *Adv. Mater.* **29** 1605448

[36] Huo C X, Cai B, Yuan Z, Ma B W and Zeng H B 2017 *Small* **1** 1600018

[37] Lai M L, Tay T Y S, Sadhanala A, Dutton S E, Li G, Friend R H and Tan Z K 2016 *J. Phys. Chem. Lett.* **7** 2653

[38] Shi Z F, Li S, Li Y, Ji H F, Li X J, Wu D, Xu T T, Chen Y S, Tian Y T, Zhang Y T, Shan C X and Du G T 2018 *ACS Nano* **12** 1462

[39] Zhang D D, Yang Y M, Bekenstein Y, Yu Y, Gibson N A, Wong A B, Eaton S W, Kornienko N, Kong Q, Lai M, Alivisatos A P, Leone S R and Yang P D 2016 *J. Am. Chem. Soc.* **138** 7236

[40] Jeon N J, Noh J H, Kim Y C, Yang W S, Ryu S and Seok S 2014 *Nat. Mater.* **13** 897

[41] Li Y, Shi Z F, Li S, Lei L Z, Ji H F, Wu D, Xu T T, Tian Y T and Li X J 2017 *J. Mater. Chem. C* **5** 8355

[42] Liu H, Zhang X W, Zhang L Q, Yin Z G, Wang D G, Meng J H, Jiang Q, Wang Y and You J B 2017 *J. Mater. Chem. C* **5** 6115

[43] Tong X W, Kong W Y, Wang Y Y, Zhu J M, Luo L B and Wang Z H 2017 *ACS Appl. Mater. Interfaces* **9** 18977

[44] Liu D, Hu Z, Hu W, Wang Y P, Yu K, Wen M, Zu Z, Liu J, Wang M, Chen W, Zhou M, Tang X and Zang Z 2017 *Mater. Lett.* **186** 243

[45] Zhang J R, Wang Q, Zhang X S, Jiang J X, Gao Z F, Jin Z W and Liu S Z 2017 *RSC Adv.* **7** 36722

[46] Liu X H, Yu D J, Cao F, Li X M, Ji J P, Chen J, Song X F and Zeng H B 2017 *Small* **13** 1700364

[47] Saidaminov M I, Haque M A, Almutlaq J, Sarmah S, Miao X H, Begum R, Zhumekenov A A, Dursun I, Cho N, Murali B, Mohammed O F, Wu T and Bakr O M 2017 *Adv. Opt. Mater.* **5** 1600704

[48] Chen Q, Zhou H, Hong Z, Luo S, Duan H S, Wang H H, Liu Y, Li G and Yang Y 2014 *J. Am. Chem. Soc.* **136** 622

[49] Wang Z W, Xu H T, Cai J, Zhu J B, Ni C W, Hong F, Fang Z B, Xu F Z, Cui S W, Xu R, Wang L J, Xu F and Huang J 2016 *Opt. Express* **24** 8411

[50] Chen Q, Zhou H, Song T B, Luo S, Hong Z, Duan H S, Dou L, Liu Y and Yang Y 2014 *Nano Lett.* **14** 4158

[51] Ying C, Shi C W, Wu N, Zhang J C and Wang M 2015 *Nanoscale* **7** 12092

[52] Li Y B, Cooper J K, Buonsanti R, Giannini C, Liu Y, Toma F M and Sharp L D 2015 *J. Phys. Chem. Lett.* **6** 493

[53] Sheng R, Ho-Baillie A, Huang S J, Chen S, Wen X M, Hao X J and Green M A 2015 *J. Phys. Chem. C* **119** 3545

[54] Zhou H, Chen Q and Yang Y 2015 *MRS Bull.* **40** 667

[55] Chen J, Fu Y P, Samad L, Dang L, Zhao Y Z, Shen S H, Guo L J and Jin S 2017 *Nano Lett.* **17** 460

[56] Zhang Q, Su R, Liu X, Xing J, Sum T C and Xiong Q H 2016 *Adv. Funct. Mater.* **26** 6238

[57] Li H L, Wang X, Zhu X L, Duan X F and Pan A L 2018 *Chem. Soc. Rev.* **47** 7504

[58] Zhou H, Yuan S P, Wang X X, Xu T, Wang X, Li H L, Zheng W H, Fan P, Li Y Y, Sun L T and Pan A L 2017 *ACS Nano* **11** 1189

[59] Liu M, Johnston M B and Snaith H J 2013 *Nature* **501** 395

[60] Malinkiewicz O, Yella A, Lee Y H, Espallargas G M, Graetzel M, Nazeeruddin M K and Bolink H J 2014 *Nat. Photon.* **8** 128

[61] Gao C, Liu J, Liao C, Ye Q Y, Zhang Y S, He X L, Guo X W, Mei J and Lau W 2015 *RSC Adv.* **5** 26175

[62] Wang S H, Ono L K, Leyden M R, Kato Y C, Raga S R, Lee M V and Qi Y B 2015 *J. Mater. Chem. A* **3** 14631

[63] Zhao D W, Ke W J, Grice R C, Cimaroli A J, Tan X X, Yang M J, Collins R W, Zhang H M, Zhu K and Yan Y F 2016 *Nano Energy* **19** 88

[64] Luo P F, Liu Z F, Xia W, Yuan C C, Cheng J G and Lu Y W 2015 *J. Mater. Chem. A* **3** 12443

[65] Peng Y K, Jing G S and Cui T H 2015 *RSC Adv.* **5** 95847

[66] Chen C W, Kang H W, Hsiao S Y, Yang P F, Chiang K M and Lin H W 2014 *Adv. Mater.* **26** 6647

[67] Dong Y H, Gu Y, Zou Y S, Song J Z, Xu L M, Li J H, Xue J, Li X M and Zeng H B 2016 *Small* **12** 5622

[68] Tang X S, Zu Z Q, Shao H B, Hu W, Zhou M, Deng M, Chen W W, Zang Z G, Zhu T and Xue J M 2016 *Nanoscale* **8** 15158

[69] Li Y, Shi Z F, Lei L Z, Ma Z Z, Zhang F, Li S, Wu D, Xu T T, Li X J, Shan C X and Du G T 2018 *ACS Photon.* **5** 2524

[70] Cha J H, Han J H, Yin W P, Park C, Park Y, Ahn T K, Cho J H and Jung D Y 2017 *J. Phys. Chem. Lett.* **8** 565

[71] Song J Z, Xu L M, Li J H, Xue J, Dong Y H, Li X M and Zeng H B 2016 *Adv. Mater.* **28** 4861

[72] Yang B, Zhang F Y, Chen J S, Yang S Q, Xia X S, Pullerits T, Deng W Q and Han K L 2017 *Adv. Mater.* **29** 1703758

[73] Pang L Q, Yao Y, Wang Q, Zhang X S, Jin Z W and Liu S Z 2018 *Part. Part. Syst. Charact.* **35** 1700363

[74] Liang J, Wang C X, Wang Y R, Xu Z R, Lu Z P, Ma Y, Zhu H F, Hu Y, Xiao C C, Yi X, Zhu G Y, Ma H L, Chen T, Tie Z X, Jin Z and Liu J 2016 *J. Am. Chem. Soc.* **138** 15829

[75] Lv L F, Xu Y B, Fang H H, Luo W J, Xu F J, Liu L M, Wang B W, Zhang X F, Yang D, Hu W D and Dong A G 2016 *Nanoscale* **8** 13589

[76] Tong G Q, Li H, Li D T, Zhu Z F, Xu E Z, Li G P, Yu L W, Xu J and Jiang Y 2018 *Small* **14** 1702523

[77] Bao C X, Yang J, Bai S, Xu W D, Yan Z B, Xu Q Y, Liu J M, Zhang W J and Gao F 2018 *Adv. Mater.* **30** 1803422

[78] Lu J W, Sheng X X, Tong G Q, Yu Z W, Sun X L, Yu L W, Xu X X, Wang J Z, Xu J, Shi Y and Chen K J 2017 *Adv. Mater.* **29** 1700400

[79] Zhou H, Zeng J P, Song Z N, Grice, C R, Chen C, Song Z H, Zhao D W, Wang H and Yan Y F 2018 *J. Phys. Chem. Lett.* **9** 2043

[80] Song Z B, Zhou H, Gui P B, Yang X H, Liu R H, Ma G K, Wang H and Fang G J 2018 *J. Mater. Chem. C* **6** 5113

[81] Jellicoe T C, Richter J M, Glass H F J, Tabachnyk M, Brady R, Dutton S E, Rao A, Friend R H, Credgington D, Greenham N C and Boehm M L 2016 *J. Am. Chem. Soc.* **138** 2941

[82] Wang A F, Guo Y Y, Muhammad F and Deng Z T 2017 *Chem. Mater.* **29** 6493

[83] Wang A, Yan X, Zhang M, Sun S, Yang M, Shen W, Pan X, Wang P and Deng Z 2016 *Chem. Mater.* **28** 8132

[84] Zhou C K, Tian Y, Yuan Z, Lin H R, Chen B H, Clark R, Dilbeck T, Zhou Y, Hurley J, Neu J, Besara T, Siegrist T, Djurovich P and Ma B W 2017 *ACS Appl. Mater. Interfaces* **9** 44579

[85] Hong W L, Huang Y C, Chang C Y, Zhang Z C, Tsai H R, Chang N Y and Chao Y C 2016 *Adv. Mater.* **28** 8029

[86] Xing G C, Kumar M H, Chong W K, Liu X F, Cai Y, Ding H, Asta M, Grätzel M, Mhaisalkar S, Mathews N and Sum T C 2016 *Adv. Mater.* **28** 8191

[87] Xu P, Chen S Y, Xiang H J, Gong X G and Wei S H 2014 *Chem. Mater.* **26** 6068

[88] Dolzhnikov D S, Wang C, Xu Y D, Kanatzidis M G and Weiss E A 2017 *Chem. Mater.* **29** 7901

[89] Jiang Y N, Zhang H L, Qiu X F and Cao B Q 2017 *Mater. Lett.* **199** 50

[90] Wong A B, Bekenstein Y, Kang J, Kley C S, Kim D, Gibson N A, Zhang D D, Yu Y, Leone S R, Wang L W, Alivisatos A P and Yang P D 2018 *Nano Lett.* **18** 2060

[91] Zhang J, Yang Y, Deng H, Farooq U, Yang X K, Khan J, Tang J and Song H S 2017 *ACS Nano* **11** 9294

[92] Singh A, Boopathi K M, Mohapatra A, Chen Y F, Li G and Chu C W 2018 *ACS Appl. Mater. Interfaces* **10** 2566

[93] Pal J, Manna S, Mondal A, Adarsh S D K V and Nag A 2017 *Angew. Chem. Int. Ed.* **56** 14187

[94] Saparov B, Hong F, Sun J P, Duan H S, Meng W W, Cameron S, Hill I G, Yan Y F and Mitzi D B 2015 *Chem. Mater.* **27** 5622

[95] Pradhan B, Kumar G S, Sain S, Dalui A, Ghorai U K, Pradhan S K and Acharya S 2018 *Chem. Mater.* **30** 2135

[96] Leng M Y, Yang Y, Zeng K, Chen Z W, Tan Z F, Li S R, Li J H, Xu B, Li D B, Hautzinger M P, Fu Y P, Zhai T Y, Xu L, Niu G D, Jin S and Tang J 2018 *Adv. Funct. Mater.* **28** 1704446

[97] Park B W, Philippe B, Zhang X L, Rensmo H, Boschloo G and Johansson E M J 2015 *Adv. Mater.* **27** 6806

[98] Yang B, Chen J S, Hong F, Mao X, Zheng K B, Yang S Q, Li Y J, Pullerits T, Deng W Q and Han K L 2017 *Angew. Chem. Int. Ed.* **56** 12471

[99] Lehner A J, Fabini D H, Evans H A, Hebert C A, Smock S R, Hu J, Wang H B, Zwanziger J W, Chabinyc M L and Seshadri R 2015 *Chem. Mater.* **27** 7137

[100] Johansson M B, Zhu H M and Johansson M J 2016 *J. Phys. Chem. Lett.* **7** 3467

[101] Zhang Y H, Yin J, Parida M R, Ahmed G H, Pan J, Bakr O M, Bredas J L and Mohammed O F 2017 *J. Phys. Chem. Lett.* **8** 3173

[102] Wu C C, Zhang Q H, Liu Y, Luo W, Guo X, Huang Z, Ting H, Sun W H, Zhong X R, Wei S Y, Wang S F, Chen Z J and Xiao L X 2018 *Adv. Sci.* **5** 1700759

[103] Slavney A H, Hu T, Lindenberg A M and Karunadasa H I 2016 *J. Am. Chem. Soc.* **138** 2138

[104] McClure E T, Ball M R, Windl W and Woodward P M 2016 *Chem. Mater.* **28** 1348

[105] Lei L Z, Shi Z F, Li Y, Ma Z Z, Zhang F, Xu T T, Tian Y T, Wu D, Li X J and Du G T 2018 *J. Mater. Chem. C* **6** 7982

[106] Wu C C, Du B W, Luo W, Liu Y, Li T Y, Wang D, Guo X, Ting H, Fang Z Y, Wang S F, Chen Z J, Chen Y X and Xiao L X 2018 *Adv. Opt. Mater.* **6** 1800811

[107] Wang P, Liu S S, Luo W J, Fang H H, Gong F, Guo N, Chen Z G, Zou J, Huang Y, Zhou X H, Wang J L, Chen X S, Lu W, Xiu F X and Hu W D 2017 *Adv. Mater.* **29** 1604439

[108] Li X M, Yu D J, Cao F, Gu Y, Wei Y, Wu Y, Song J Z and Zeng H B 2016 *Adv. Funct. Mater.* **26** 5903

[109] Cao F, Yu D J, Li X M, Zhu Y, Sun Z G, Shen Y L, Wu Y, Wei Y and Zeng H B 2017 *J. Mater. Chem. C* **5** 7441

[110] Ramasamy P, Lim D H, Kim B, Lee S H, Lee M S and Lee J S 2016 *Chem. Commun.* **52** 2067

[111] Waleed A, Tavakoli M M, Gu L L, Hussain S, Zhang D Q, Poddar S, Wang Z Y, Zhang R J and Fan Z Y 2017 *Nano Lett.* **17** 4951

[112] Song J Z, Cui Q Z, Li J H, Xu J Y, Yang Y, Xu L M, Dong Y H, Tian T, Sun H D and Zeng H B 2017 *Adv. Opt. Mater.* **5** 1700157

[113] Li X M, Yu D J, Chen J, Wang Y, Cao F, Wei Y, Wu Y, Wang L, Zhu Y, Sun Z G, Ji J P, Shen Y L, Sun H D and Zeng H B 2017 *ACS Nano* **11** 2015

[114] Li C L, Han C, Zhang Y B, Zang Z G, Wang M and Tang X S 2017 *Sol. Energ. Mat. Sol. C.* **172** 341

[115] Zhang X S, Wang Q, Jin Z W, Zhang J R and Liu S Z 2017 *Nanoscale* **9** 6278

[116] Song X F, Liu X H, Yu D J, Huo C X, Ji J P, Li X M, Zhang S L, Zou Y S, Zhu G Y, Wang Y J, Wu M Z, Xie A and Zeng H B 2018 *ACS Appl. Mater. Interfaces* **10** 2801